Published in final edited form as:
IEEE Trans Ultrason Ferroelectr Freq Control. 2011 November ; 58(11): 2334–2343. doi:10.1109/TUFFC.2011.2091.

Lesion Generation Through Ribs Using Histotripsy Therapy Without Aberration Correction

Yohan Kim, **Tzu-Yin Wang**, **Zhen Xu[Member, IEEE]**, and **Charles A. Cain[Fellow, IEEE]**
University of Michigan, Department of Biomedical Engineering, Ann Arbor, MI

Yohan Kim: yohankim@umich.edu

Abstract

This study investigates the feasibility of using high-intensity pulsed therapeutic ultrasound, or histotripsy, to non-invasively generate lesions through the ribs. Histotripsy therapy mechanically ablates tissue through the generation of a cavitation bubble cloud, which occurs when the focal pressure exceeds a certain threshold. We hypothesize that histotripsy can generate precise lesions through the ribs without aberration correction if the main lobe retains its shape and exceeds the cavitation initiation threshold and the secondary lobes remain below the threshold. To test this hypothesis, a 750-kHz focused transducer was used to generate lesions in tissue-mimicking phantoms with and without the presence of rib aberrators. In all cases, 8000 pulses with 16 to 18 MPa peak rarefactional pressure at a repetition frequency of 100 Hz were applied without aberration correction. Despite the high secondary lobes introduced by the aberrators, high-speed imaging showed that bubble clouds were generated exclusively at the focus, resulting in well-confined lesions with comparable dimensions. Collateral damage from secondary lobes was negligible, caused by single bubbles that failed to form a cloud. These results support our hypothesis, suggesting that histotripsy has a high tolerance for aberrated fields and can generate confined focal lesions through rib obstacles without aberration correction.

I. Introduction

The effects of acoustic obstruction from rib bones have long been a challenge to researchers in high-intensity focused ultrasound (HIFU). In several non-invasive surgery applications, such as treatment for liver and pancreatic cancer, it is often the case that the available acoustic windows are partially blocked by the ribs, which can substantially decrease the ultrasound energy delivery to the focal target and may overheat overlying tissues because of the highly absorptive nature of bones [1]–[4]. Furthermore, ribs can generate significant field aberration, resulting in increased secondary lobes and reduced main lobe intensities in the beam profile, which may cause undesired collateral damage.

To overcome these issues, considerable efforts have been dedicated to develop aberration correction algorithms to spare the ribs and improve beam forming. Theoretical studies on the application of virtual phased arrays to sonicate between the rib bones have been conducted [5]; a physically segmented transducer design was also proposed to prevent sonication to the ribs by aligning active elements with the intercostal gaps [6]. More recently, adaptive focal optimization algorithms for transcostal therapy have been developed, depending on the presence of a point source or an identifiable acoustic spot at the desired focus [7], [8]. More sophisticated non-invasive approaches using ultrasound scanning and time-reversal to identify the ribs [9] require transducers with transmit and receive capabilities. Other non-invasive methods involve the use of computed tomography or magnetic resonance imaging [10], [11] to image the rib obstructions and selectively deactivate elements shadowed by the rib bones.

Even if the ribs are spared, another potential issue is the formation of strong secondary lobes at the focal profile caused by the spatial distribution of the ribs. This focal splitting effect has been described and characterized more analytically in a recent study [12], which shows that secondary lobes may still be present in the focal profile even after correction algorithms are applied because of the periodic ultrasound blockage pattern caused by the ribs.

This paper presents our investigation on the feasibility of using histotripsy therapy to generate lesions through rib aberrators without applying any correction mechanisms other than transducer power modulation to compensate for attenuation effects. Histotripsy uses controlled cavitation bubble clouds to induce mechanical tissue fractionation. The bubble clouds are produced by using short (<20 μs), high-pressure (peak rarefactional pressure >10 M Pa) shockwave ultrasound pulses at a low duty cycle, typically <5% [13]–[15], minimizing thermal effects [16]. Based on the high echogenicity of cavitating bubble clouds, treatment can also be readily monitored in real time using any conventional ultrasound imaging system, allowing the operator to recognize whether cavitation bubble clouds have been generated.

The tissue fractionation effect from histotripsy therapy occurs when the focal pressure exceeds a certain threshold level at which a cavitation bubble cloud is initiated [17]–[19]. Based on this threshold mechanism, we hypothesize that histotripsy therapy can generate precise lesions through the ribs, provided that the pressure main lobe maintains its shape and exceeds the bubble cloud initiation threshold and secondary lobes remain below the threshold (Fig. 1). No bubble clouds are generated in regions that are below the initiation threshold, resulting in minimal collateral damage to regions surrounding the main lesion.

To test our hypothesis, histotripsy treatment was applied to tissue-mimicking gel phantoms in a free field and through rib aberrators at similar rarefactional focal pressures and identical treatment settings without using aberration correction. The bubble cloud generated was monitored for cases with and without the rib aberrators, and the resulting lesions were compared for overall dimensions and presence of collateral damage caused by secondary lobes.

II. Materials and Methods

A. Therapeutic Transducer

A 750-kHz, 18-channel spherically focused transducer (Imasonic, Voray sur l’Ognon, France) was used in this study. The transducer has a geometric focal length of 12 cm, with an aperture size of 15 cm (f/number 0.8) and a 5.9-cm-diameter center hole designed to accommodate an ultrasound imaging probe (not used in this study). All 18 elements were driven in phase through a custom-designed 18-channel switching amplifier unit with appropriate electrical matching circuits built in our laboratory. Input signal controls were provided by a field-programmable gate array (FPGA) board (Altera Corporation, San Jose, CA) that functioned as a custom signal generator.

B. Experimental Apparatus

A rib phantom made of polycarbonate rods was constructed to emulate acoustic aberration conditions typically caused by rib bones. The rods had a diameter of 13 mm and were separated by 25 to 30 mm, which are comparable to the sizes and intercostal separations in the human ribcage. In addition to the polycarbonate rib phantom, excised ribcage sections from adult pigs were also used for further validation. Both the phantom and the rib sections were positioned between the transducer and its geometric focus inside a tank filled with degassed water. Porcine rib sections were immersed in a thin plastic bag with 0.9% saline, and then submerged in the tank. An illustration of the experiment setup is given in Fig. 2.

A high-sensitivity needle hydrophone (HNR-0500 Onda Corp., Sunnyvale CA) was used to scan focal pressure profiles with and without the rib aberrators. Pressure profiles were obtained for each of the situations considered in this study: in a free field, with the rib phantom positioned at 8 and 4 cm from the focus, and with porcine ribs at 8 cm from the focus. At the focus, high-pressure shockwave measurements were conducted using a multimode fiber optic hydrophone system designed and built in-house [20]. Based on these high-pressure measurements, the peak rarefactional pressure was controlled so that it would be approximately equal at the focus for all treatments.

C. Bubble Cloud Imaging

A high-speed, 1-megapixel CCD camera, (Phantom V210, Vision Research, Wayne, NJ) was used to capture images of bubble clouds in transparent 1% agarose gel phantoms with and without the rib aberrators. The camera was triggered through the same FPGA signal generator driving the transducer's amplifier system. Images of the bubble cloud were collected at a set delay of 12 μs after each pulse's arrival at the transducer's geometric focus, with one frame (1280 × 800 pixels) captured every 10 treatment pulses (800 frames captured per treatment). A back-lit setup was used with a halogen light source, intensified with Fresnel lens sheets. An adjustable camera lens (AF Nikkor 70 to 210 mm, f/number 4 to 5.6; Nikon, Tokyo, Japan) coupled with magnifying lenses allowed an image resolution of 40 pixels/mm. To achieve satisfactory background illumination through the gel phantom, frame exposure times were set at 4 μs.

D. Red Blood Cell Phantom Treatment

Tissue-mimicking red blood cell (RBC) agarose phantoms developed in our laboratory were used to assess the extent of the fractionation produced with and without the presence of the rib aberrators. The base composition of the gel phantom was made by mixing agarose power and saline (0.9%) at a ratio of 1% of agarose to saline by weight. Structurally, the phantoms consisted of three layers, with the top and bottom layers (2 to 2.5 cm in thickness) acting as buffer zones between the water in the tank and the middle (RBC) layer (approximately 0.5 to 1.5 mm in thickness), in which canine RBCs (5% concentration by volume) were added. The phantom has been successfully used as an indicator of cavitational damage caused by histotripsy in tissue [21]. The opaque, intact RBC layer in the phantom becomes translucent once the cells in the layer are fractionated by cavitation [Fig. 3(a)]. The major advantage of using RBC phantoms over tissue is that cell fractionation patterns caused by histotripsy treatment can be visualized directly in different planes without time-consuming histopathological analysis.

Treatment was administered through the rib aberrators by driving the transducer in such a way that the peak rarefactional pressure at the focus was equivalent to that applied in free-field treatments. For each case, treatment pulses were applied at a pulse repetition frequency (PRF) of 100 Hz and 5 cycles per pulse. A total of 8000 pulses were applied per treatment (80 s) to ensure complete fractionation of the targeted volume.

Lesion profiles were created along the transversal and longitudinal focal planes by appropriately positioning the RBC layer at the focal zone. For transversal lesions, the RBC layer was positioned perpendicularly with respect to the axis of the transducer. Longitudinal plane lesions were generated by positioning the RBC layer at the focus, parallel to the axis of the transducer.

Lesion sizes and collateral damage distribution were assessed with the aid of an image analysis script written in-house [22]. The script allows image binarization into fractionated and intact areas, with fractionated areas defined as zones with pixel intensities three standard

deviations higher than the chosen background, typically the space-averaged intensity of pixels from a sample area on the intact blood layer. Once the image is binarized, lesion dimensions are then estimated by a pixel count. For this study's purpose, the continuous translucent area extending from the center of the main lobe location was defined as the main lesion, and collateral damage was defined as the remaining damage spots found outside the main lesion [Fig. 3(b)].

III. Results

A. Acoustic Pressure Profile

Without applying power compensation, the presence of the rib aberrators substantially reduced the peak rarefactional pressure amplitude at the focus in comparison to free-field measurements. Pressure insertion losses were approximately −5.5 dB through the rib phantom and up to −7 dB through the porcine ribs. High levels of secondary (grating) lobes were introduced in the focal profile along the transversal axis perpendicular to the orientation of the rib obstacles. No significant secondary lobe development was observed in the transversal axis parallel to the orientation of the obstacles or along the longitudinal axis of propagation. The highest secondary lobes were in the range of −7 to −4 dB normalized to their respective main lobes; −7 dB with porcine ribs and −4 dB with the rib phantom positioned at 4 cm from the focus (Fig. 4). The location of the secondary lobes varied from 5 to 8 mm with respect to the center of the main lobe, developing closer to the center when the rib obstacles were placed farther away from the transducer (closer to the focus).

In comparison to free-field measurements, the main lobe did not undergo any noticeable shift in the transversal or longitudinal coordinates in the presence of the rib phantom. In scans involving the porcine ribs, the main lobe was shifted closer toward the transducer by approximately 3 mm, but no significant transversal shifts were observed. Despite the presence of high secondary lobes, the main lobe remained undistorted in all cases.

The measured minimum focal pressure threshold to initiate and maintain a cavitation bubble cloud in degassed water (40 to 45% dissolved O_2) under free-field conditions was approximately at a peak rarefactional pressure of 16 M Pa and a peak compressional pressure of 60 M Pa (with 5-cycle pulses delivered at a 100 Hz repetition rate). Because of the significant insertion losses measured in the presence of the rib aberrators, the transducer power was appropriately increased to compensate for the attenuation and approximately equalize peak rarefactional pressure levels at the focus, which were within the range of 16 to 18 MPa (Fig. 5).

B. Bubble Cloud Imaging

Cavitation bubble clouds of comparable sizes were successfully developed at the focus in all cases, with and without the rib aberrators. In the initial stages of the treatment, large bubbles were observed to form at the location of the main lobe within the first few pulses. These cavitation bubbles eventually formed a larger cigar-shaped bubble cloud at the location of the main lobe as the gel was fractionated (Fig. 6).

In the presence of the rib obstacles, small cavitation nuclei were also observed near locations where the secondary lobes were the highest. However, as treatment progressed, these marginal bubbles did not become part of a cloud and were pushed away by radiation force, eventually collapsing on their own within the first 1000 to 2000 pulses.

C. Lesion and Collateral Damage Analysis

Lesions were successfully created at the focus of the transducer in all cases. A total of 87 lesions were created in RBC phantoms: 22 reference lesions were generated under free-field conditions, 45 lesions were created through the polycarbonate rib phantom, and 20 lesions were created through the porcine ribs. Morphology of representative transversal plane lesions is shown in Fig. 7. A circular main lesion was observed in all treatment cases, with collateral damage occurring in the form of a few sporadic points within a ring shaped zone around the main lesion area. In treatments through the rib aberrators, minor damage spots were observed at the locations where the secondary lobes were the highest, but no significant fractionation areas were observed outside the main lesion.

To evaluate the longitudinal plane lesion profiles, the RBC tissue phantom was positioned in such a way that the RBC layer was perpendicular with respect to the orientation of the rib obstacles to ensure that the layer co-incided with the plane where the secondary lobes were present. A cigar shaped main lesion was created in all treatments, with incompletely fractionated areas in the form of thin damage streaks at the tail of the main lesion (Fig. 8). Lesions generated through the rib aberrators also displayed damage streaks on both sides of the main lesion, consistent with locations where the temporary marginal nuclei were observed during the high-speed camera imaging. However, as with the transversal plane treatments, no significant lesion development occurred outside the main lobe region.

In a more quantitative point of view, the focal lesion areas generated through the rib aberrators were comparable to within a standard deviation of the lesion areas created in a free field, although the mean lesion sizes generated through the aberrators were slightly smaller (Fig. 9). Considering mean lesion dimensions in both transversal and longitudinal planes, the largest lesions were generated in free-field conditions, whereas the smallest lesions were obtained through the porcine ribs.

The collateral damage created through the porcine ribs was minimal and not statistically significant in comparison to that observed in free-field lesions (transversal: $N = 10$, P-value = 0.92; longitudinal: $N = 10$, P-value = 0.7). Higher levels of collateral damage from marginal bubble nuclei were observed in lesions created through the rib phantom, particularly when the phantom was placed closer to the focus (at 4 cm).

In actual treatment scenarios, it is likely that a region larger than a single focal size will need to be ablated. Lesions consisting of 5 focal spots separated by 1 mm were created by mechanically scanning the transducer to examine the feasibility of generating composite lesions through the ribs (Fig. 10). As with the single-focus treatments, comparable fractionated areas were created in all cases; lesion development was well confined and limited to the focal zone, whereas collateral damage from secondary lobes consisted of thin streaks caused by the translation of marginal bubble nuclei.

IV. Discussion

The rib aberrators significantly distorted the focal profile in the form of increased secondary lobes at the expense of reduced main lobe intensities in comparison to free-field measurements. In this case, the formation of secondary lobes is primarily a consequence of the distribution of the solid bone obstacles in the ribs, which together act as an acoustically diffractive mask, effectively creating an aperture with active elements radiating from the intercostal separations between the solid obstacles. It has been shown theoretically [23] that although the relative location of these secondary lobes (in this case, grating lobes) may change depending on the spatial pattern of the distribution of the rib bones, the main lobe should remain relatively undistorted if a reasonably large transducer aperture is used. This is

consistent with our measurements; the main lobe profile did not appear to be appreciably changed (except for attenuation effects) with the introduction of the rib aberrators. Other forms of acoustic aberration may affect the beam profiles similarly [24], so this method may be relevant to other situations in which acoustic aberration effects limit therapeutic options, e.g.: the skull.

We hypothesized that histotripsy therapy could be used to generate precise lesions through the ribs, as long as the focal main lobe maintains its shape and exceeds the cavitation cloud initiation threshold and the secondary lobes remain below the threshold. Supporting our premise, cavitation bubble clouds of similar sizes were generated through the ribs, and despite the high secondary lobes introduced by the rib aberrators, the formation of a bubble cloud was limited to the main lobe, which was also the only location where a full lesion successfully developed. Temporary cavitation bubbles were observed to form at the locations of secondary lobes during the initial stages of treatment through the rib aberrators, but these bubbles did not form a cloud, eventually collapsing on their own, pushed away by radiation force. This is evidenced by the collateral damage patterns observed in the RBC phantoms, which consisted of peripheral spots or streaks not comparable to the central main lesion.

It is interesting to note that the secondary lobe levels measured through the porcine ribs were lower than those measured through the polycarbonate rib phantom. One plausible explanation is that the more uniform geometry of the phantom created better conditions for the formation of secondary lobes at the focal profile in comparison to the relatively randomly shaped and spaced porcine ribs. As a consequence, lesions created through the porcine ribs were more confined, presenting minimal collateral damage in comparison to lesions generated in the free field. In clinical applications requiring a larger volume to be ablated, lesions with multiple foci could be generated by mechanically sweeping the focus of the transducer (as shown in this paper) or by electronic focal steering if a phased array is used. For larger ablated regions, it is expected that the collateral damage caused by secondary lobes would become even less relevant relative to the total size of the lesion.

Although the main lesion dimensions generated with and without the rib aberrators were comparable when using standard deviation ranges, the mean area of lesions obtained through the rib aberrators was smaller than free-field lesions—a result that may seem counter-intuitive because similar treatment parameters were used. It should be pointed out, however, that although all lesions were generated at comparable focal peak rarefactional pressure levels, (16 to 18 M Pa) peak compressional pressures were observed to vary more significantly, with measurements differing by as much as 25 M Pa in comparison with the free field. Peak rarefactional pressure measurements have been commonly reported in literature as thresholds for cavitation events [25]–[27], but a recent study from our laboratory has shown evidence that peak compressional pressures (higher-pressure harmonics) play a significant role in the inception of a cavitation bubble cloud in the pulsed ultrasound regime used in histotripsy therapy [19]. It is possible that the attenuation of these higher-pressure harmonics may have affected the cavitation dynamics at the focus, resulting in the formation of smaller lesions in the presence of the rib aberrators. This correlates with the observation that the smallest lesions were generated through the porcine ribs and through the rib phantom positioned at 4 cm from the focus, which were also the configurations that most attenuated the focal peak compressional pressure levels.

From this perspective, it is noticeable that the peak compressional pressure measured through the porcine ribs was considerably lower than its counterparts in the free field and through the polycarbonate rib phantom (up to 35%), but no comparable reduction in the sizes of the bubble clouds or lesions were observed. In this particular case, the peak

compressional pressure may have been underestimated because the focal pressure measurements were taken at the geometric focus of the transducer. As previously noted, the porcine ribs introduced a small axial shift (3 mm) in the focal profile. Because the higher harmonic components of a shockwave have much tighter focusing characteristics than the fundamental, the focal shift may have significantly lowered the peak compressional pressure amplitude measured at the geometric focus of the transducer.

Although cavitation threshold pressures cannot be easily measured *in vivo*, histotripsy therapy at or near bubble cloud threshold levels is still feasible because cavitation bubble clouds can be readily monitored using conventional ultrasound imagers, allowing the operator to be aware of when and where the threshold has been reached anywhere within a given region of interest. In an *in vivo* scenario, the operator would start the treatment from low acoustic power settings and gradually increase power levels until a cavitation bubble cloud is imaged at the focal spot. Once a bubble cloud is created at the focus, treatment could then proceed at that level, confining the bubble cloud to the location of the main lobe and preventing secondary lobes from reaching the cavitation threshold. This provides direct imaging feedback to validate the location of the tissue ablating bubble cloud.

In addition, because cavitation bubble clouds can be initiated at arbitrarily low duty cycles—even single pulses—as long as enough pressure is available at the focus, the likelihood of inducing thermal effects in overlying tissues can be drastically reduced with the pulsed ultrasound parameters used in histotripsy therapy. In this study, for example, the effective sonication duty cycle applied to achieve a bubble cloud was less than 0.07% in all treatments, which is virtually negligible in terms of HIFU therapy standards. This could potentially allow transcostal therapy to be performed by simple single-element transducers with minimal thermal effects on the ribs, without requiring phased-array designs to sonicate between the intercostal spaces. Thus, with a sufficiently powerful transducer, compensation of the main lobe pressure to counter-act attenuation could be accomplished without significant thermal consequences to overlying tissues at the expense of reduced duty cycle, and perhaps, treatment time.

Although in this study histotripsy therapy was applied to create lesions through rib obstacles without any compensation methods other than power modulation, aberration correction mechanisms may be beneficial to help improve focusing and increase treatment efficiency, especially when severe phase aberration is present. Potential sources of phase aberration are multiple layers of thick inhomogeneous tissue, which could significantly distort the main lobe and prevent the initiation of a cavitation bubble cloud at the focus. Because it is only necessary to move the peak pressure of the focal main lobe beyond the bubble cloud cavitation threshold and above all secondary lobes, relatively coarse aberration correction schemes could potentially be applied to appropriately accentuate the main lobe, if necessary. Future studies will explore how such inhomogeneous tissue may affect histotripsy therapy, followed by an investigation of possible methods to circumvent aberration effects and improve the efficacy of the treatment.

V. Conclusions

This study evaluated the feasibility of using histotripsy therapy to generate lesions through rib obstacles without using aberration correction mechanisms. We hypothesized that precise lesions can be generated through ribs by histotripsy therapy without aberration correction as long as the pressure main lobe maintains its shape and exceeds the cavitation cloud initiation threshold and secondary lobes remain below the threshold.

The rib aberrators significantly attenuated the peak focal pressure and introduced high secondary lobes in the focal profile. Treatment was conducted by adjusting the input voltage

of the transducer such that the peak rarefactional pressures at the focus were at levels similar to free-field conditions. Despite the presence of significant secondary lobes, cavitation bubble clouds were observed to develop exclusively at the main lobe locations, resulting in lesions that were comparable in size to those created under free-field conditions. Collateral damage from secondary lobes was limited to damage spots caused by temporary cavitation bubbles that failed to form a cloud.

The threshold nature of the bubble cloud initiation in histotripsy therapy appears to confer a high degree of robustness to the bubble cloud shape in the presence of secondary lobes introduced by rib aberrators. This characteristic, coupled with the non-thermal nature of the treatment, suggest that histotripsy therapy could be a useful non-invasive tissue ablation modality for transcostal surgical applications such as treatment for hepatic and pancreatic cancer, or for cardiac ablation procedures.

Acknowledgments

This work is supported by NIH grants R01 EB008998, R01 EB007643, and R01 CA134579; NSF grant S10 RR022425; and The Hartwell Foundation.

The authors thank Dr. K. Ives for her help in obtaining the tissue samples used in the experiments, as well as A. Maxwell for his helpful suggestions and discussions on various aspects of the project.

References

1. Wu F, Wang ZB, Chen WZ, Wang W, Gui Y, Zhang M, Zheng G, Zhou Y, Xu G, Li M, Zhang C, Ye H, Feng R. Extracorporeal high intensity focused ultrasound ablation in the treatment of 1038 patients with solid carcinomas in China: An overview. Ultrason Sonochem. May.2004 11:149–154. [PubMed: 15081972]
2. Kennedy JE, Wu F, ter Haar GR, Gleeson FV, Phillips RR, Middleton MR, Cranston D. High-intensity focused ultrasound for the treatment of liver tumours. Ultrasonics. Apr.2004 42:931–935. [PubMed: 15047409]
3. Jung SE, Cho SH, Jang JH, Han JY. High-intensity focused ultrasound ablation in hepatic and pancreatic cancer: Complications. Abdom Imaging. 2010; 36(2):185–195. [PubMed: 20512487]
4. Li JJ, Xu GL, Gu MF, Luo GY, Rong Z, Wu PH, Xia JC. Complications of high intensity focused ultrasound in patients with recurrent and metastatic abdominal tumors. World J Gastroenterol. May 21.2007 13:2747–2751. [PubMed: 17569147]
5. Botros YY, Ebbini ES, Volakis JL. Two-step hybrid virtual array ray (VAR) technique for focusing through the rib cage. IEEE Trans Ultrason Ferroelectr Freq Control. 1998; 45(2):989–1000. [PubMed: 18244253]
6. Civale J, Clarke R, Rivens I, ter Haar G. The use of a segmented transducer for rib sparing in HIFU treatments. Ultrasound Med Biol. Nov.2006 32:1753–1761. [PubMed: 17112961]
7. Aubry JF, Pernot M, Marquet F, Tanter M, Fink M. Transcostal high-intensity-focused ultrasound: Ex vivo adaptive focusing feasibility study. Phys Med Biol. Jun 7.2008 53:2937–2951. [PubMed: 18475006]
8. Ballard JR, Casper AJ, Wan Y, Ebbini ES. Adaptive transthoracic refocusing of dual-mode ultrasound arrays. IEEE Trans Biomed Eng. Jan.2010 57:93–102. [PubMed: 19651547]
9. Cochard E, Prada C, Aubry JF, Fink M. Ultrasonic focusing through the ribs using the DORT method. Med Phys. Aug.2009 36:3495–3503. [PubMed: 19746783]
10. Liu HL, Hsu CL, Huang SM, Hsi YW. Focal beam distortion and treatment planning for transrib focused ultrasound thermal therapy: A feasibility study using a two-dimensional ultrasound phased array. Med Phys. Feb.2010 37:848–860. [PubMed: 20229894]
11. Quesson B, Merle M, Kohler MO, Mougenot C, Roujol S, de Senneville BD, Moonen CT. A method for MRI guidance of intercostal high intensity focused ultrasound ablation in the liver. Med Phys. Jun.2010 37:2533–2540. [PubMed: 20632565]

12. Bobkova S, Gavrilov L, Khokhlova V, Shaw A, Hand J. Focusing of high-intensity ultrasound through the rib cage using a therapeutic random phased array. Ultrasound Med Biol. Jun.2010 36:888–906. [PubMed: 20510186]
13. Parsons JE, Cain CA, Abrams GD, Fowlkes JB. Pulsed cavitational ultrasound therapy for controlled tissue homogenization. Ultrasound Med Biol. Jan.2006 32:115–129. [PubMed: 16364803]
14. Hall TL, Kieran K, Ives K, Fowlkes JB, Cain CA, Roberts WW. Histotripsy of rabbit renal tissue in vivo: Temporal histologic trends. J Endourol. Oct.2007 21:1159–1166. [PubMed: 17949317]
15. Kim Y, Gelehrter SK, Fifer CG, Lu JC, Owens GE, Berman DR, Williams J, Wilkinson JE, Ives KA, Xu Z. Non-invasive pulsed cavitational ultrasound for fetal tissue ablation: Feasibility study in a fetal sheep model. Ultrasound Obstet Gynecol. 2011; 37(4):450–457. [PubMed: 21433165]
16. Kieran K, Hall TL, Parsons JE, Wolf JS Jr, Fowlkes JB, Cain CA, Roberts WW. Refining histotripsy: Defining the parameter space for the creation of nonthermal lesions with high intensity, pulsed focused ultrasound of the in vitro kidney. J Urol. Aug.2007 178:672–676. [PubMed: 17574617]
17. Xu Z, Fowlkes JB, Ludomirsky A, Cain CA. Investigation of intensity thresholds for ultrasound tissue erosion. Ultrasound Med Biol. Dec.2005 31:1673–1682. [PubMed: 16344129]
18. Xu Z, Fowlkes JB, Rothman ED, Levin AM, Cain CA. Controlled ultrasound tissue erosion: The role of dynamic interaction between insonation and microbubble activity. J Acoust Soc Am. Jan. 2005 117:424–435. [PubMed: 15704435]
19. Maxwell, AD.; Tzu-Yin, W.; Cain, CA.; Fowlkes, JB.; Zhen, X.; Sapozhnikov, OA.; Bailey, MR. The role of compressional pressure in the formation of dense bubble clouds in histotripsy. IEEE Int. Ultrasonics Symp; Sep. 20–23, 2009; p. 81-84.
20. Parsons JE, Cain CA, Fowlkes JB. Cost-effective assembly of a basic fiber-optic hydrophone for measurement of high-amplitude therapeutic ultrasound fields. J Acoust Soc Am. Mar.2006 119:1432–1440. [PubMed: 16583887]
21. Maxwell AD, Wang TY, Yuan L, Duryea AP, Xu Z, Cain CA. A tissue phantom for visualization and measurement of ultrasound-induced cavitation damage. Ultrasound Med Biol. Dec.2010 36:2132–2143. [PubMed: 21030142]
22. Wang TY, Xu Z, Hall T, Fowlkes J, Roberts W, Cain C. Active focal zone sharpening for high-precision treatment using histotripsy. IEEE Trans Ultrason Ferroelectr Freq Control. Feb.2011 58:305–315. [PubMed: 21342816]
23. Khokhlova V, Bobkova S, Gavrilov L. Focus splitting associated with propagation of focused ultrasound through the rib cage. Acoust Phys. 2010; 56(5):665–674. [PubMed: 21607120]
24. Hong W, Ebbini ES, O'Donnell M, Cain CA. Phase aberration correction and motion compensation for ultrasonic hyperthermia phased arrays: Experimental results. IEEE Trans Ultrason Ferroelectr Freq Control. 1994; 41(1):34–43.
25. Fowlkes JB, Crum LA. Cavitation threshold measurements for microsecond length pulses of ultrasound. J Acoust Soc Am. Jun.1988 83:2190–2201. [PubMed: 3411016]
26. Holland CK, Apfel RE. Thresholds for transient cavitation produced by pulsed ultrasound in a controlled nuclei environment. J Acoust Soc Am. Nov.1990 88:2059–2069. [PubMed: 2269722]
27. Coleman AJ, Kodama T, Choi MJ, Adams T, Saunders JE. The cavitation threshold of human tissue exposed to 0.2-MHz pulsed ultrasound: Preliminary measurements based on a study of clinical lithotripsy. Ultrasound Med Biol. 1995; 21(3):405–417. [PubMed: 7645132]

Biographies

Yohan Kim is a graduate student in the Department of Biomedical Engineering at the University of Michigan, Ann Arbor. He received his B.S. degree in 2006 from the University of Texas at Austin and his M.S. degree in 2009 from the University of Michigan, Ann Arbor, both in electrical engineering. He has been part of the Biomedical Ultrasound Laboratory, where he is currently pursuing his Ph.D. degree, since 2008. His research interests include noninvasive ultrasound surgery, therapeutic transducer design, and high-power control electronics for piezoelectric transducers.

Tzu-Yin Wang is a graduate student in the Department of Biomedical Engineering at the University of Michigan, Ann Arbor, MI. She received her B.S. and M.S. degrees, both in electrical engineering, from the National Taiwan University, Taipei, Taiwan, in 2004 and 2006, respectively. Her research interests include ultrasound therapy control and monitoring, mechanisms of cavitation-induced tissue fractionation, and phased-array ultrasound transducers for therapeutics.

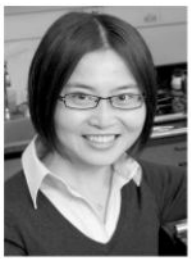

Zhen Xu (S’05–M’06) is an Assistant Professor in the Department of Biomedical Engineering at the University of Michigan, Ann Arbor, MI. She received the B.S.E. (highest honors) degree in biomedical engineering from Southeast University, Nanjing, China, in 2001, and her M.S. and Ph.D. degrees from the University of Michigan in 2003 and 2005, respectively, both in biomedical engineering. Her research is focused on ultrasound therapy, particularly the applications of histotripsy for noninvasive surgeries. In 2006, she received the IEEE Ultrasonics, Ferroelectrics, and Frequency Control Society’s Outstanding Paper Award.

Charles A. Cain (S'65–M'71–SM'80–F'89) was born in Tampa, FL, on March 3, 1943. He received the B.E.E. (highest honors) degree in 1965 from the University of Florida, Gainesville, FL; the M.S.E.E. degree in 1966 from the Massachusetts Institute of Technology, Cambridge, MA; and the Ph.D. degree in electrical engineering in 1972 from the University of Michigan, Ann Arbor, MI. From 1965 through 1968, he was a member of the Technical Staff at Bell Laboratories, Naperville, IL, where he worked in the area of electronic switching systems development. From 1972 through 1989, he was in the Department of Electrical and Computer Engineering at the University of Illinois at Urbana-Champaign, where he was a professor of electrical engineering and bioengineering. Since 1989, he has been in the College of Engineering at the University of Michigan, Ann Arbor, as a professor of biomedical engineering and electrical engineering. He was the chair of the Biomedical Engineering Program from 1989 to 1996, the founding chair of the Biomedical Engineering Department from 1996 to 1999, and the Richard A. Auhll Professor of Engineering in 2002. He has been involved in research on the medical applications of ultrasound, particularly highintensity ultrasound for noninvasive surgery. He was formerly an associate editor of the *IEEE Transactions on Biomedical Engineering* and the *IEEE Transactions on Ultrasonics, Ferroelectrics, and Frequency Control* and an editorial board member of the *International Journal of Hyperthermia and Radiation Research*. He is a fellow of the IEEE and the American Institute for Medical and Biological Engineering (AIMBE).

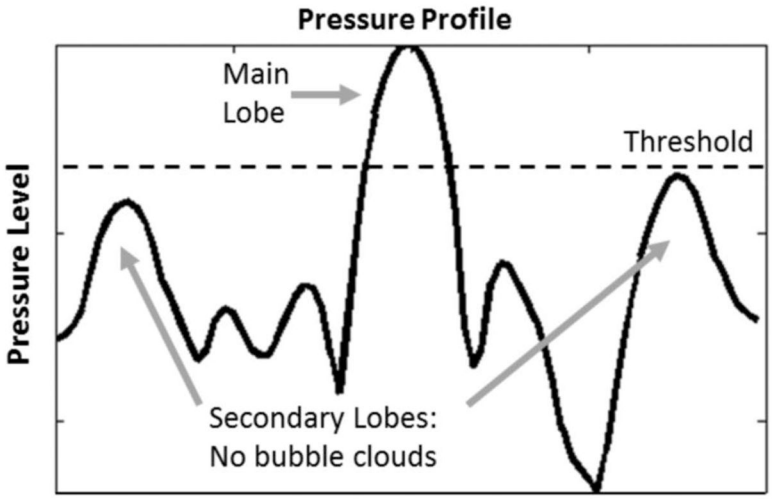

Fig. 1.

Illustration of the cavitation threshold effect in histotripsy therapy: By modulating the acoustic power in such a way that only the main lobe exceeds the bubble cloud initiation threshold, confined focal lesions with minimal collateral damage should be generated at the treatment focus.

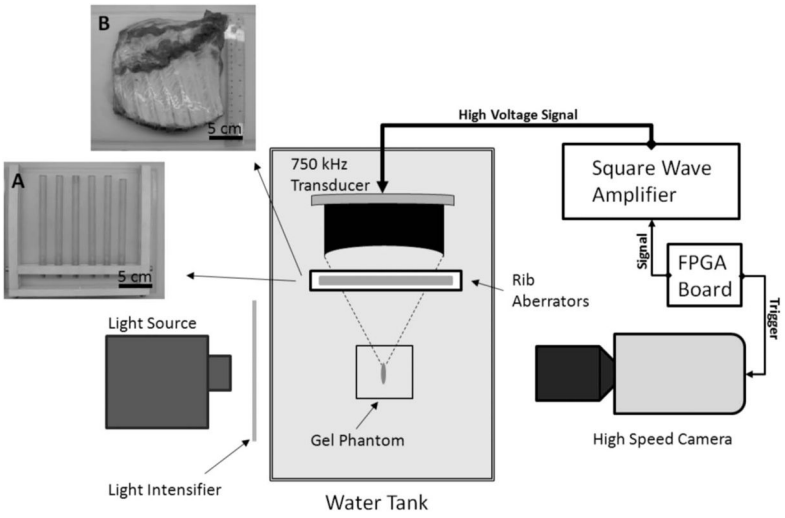

Fig. 2.

Illustration of the experimental setup for bubble cloud imaging with pictures of the rib aberrators: A = polycarbonate rib phantom, B = porcine rib section.

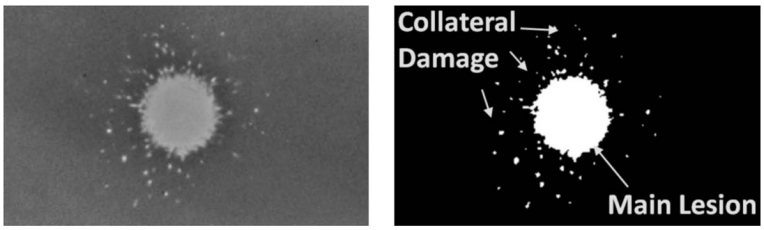

Fig. 3.
(a) Sample picture of a treated red blood cell phantom showing a translucent lesion. (b) Processed image sample for lesion size and collateral damage assessment. Collateral damage appears as small damage spots surrounding the main lesion area.

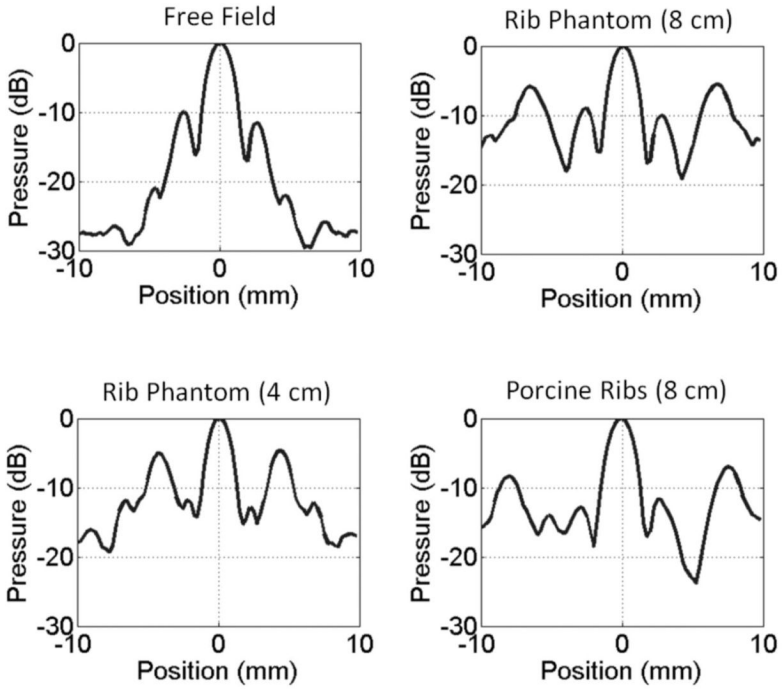

Fig. 4.

Normalized transversal focal pressure profiles obtained in a free field and through the rib aberrators. Secondary lobes were not observed to develop in the longitudinal axis or the transversal axis parallel to the orientation of the rib obstacles. Rib Phantom (8 cm) indicates that the rib phantom was placed between the transducer and the focus, 8 cm away from the focus. Scan profiles reference peak rarefactional values at each location.

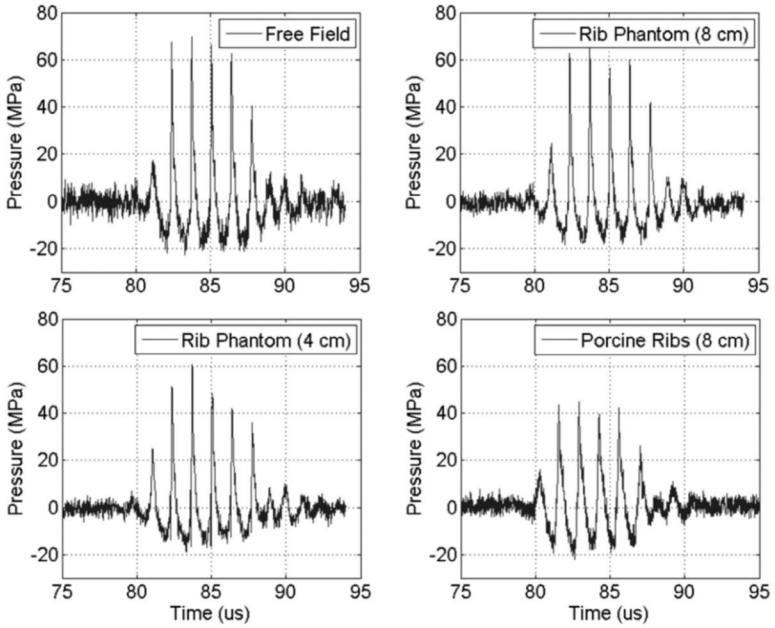

Fig. 5.

Treatment pulse waveforms measured in a free field and through the rib aberrators. Measurements taken at the geometric focus of the transducer.

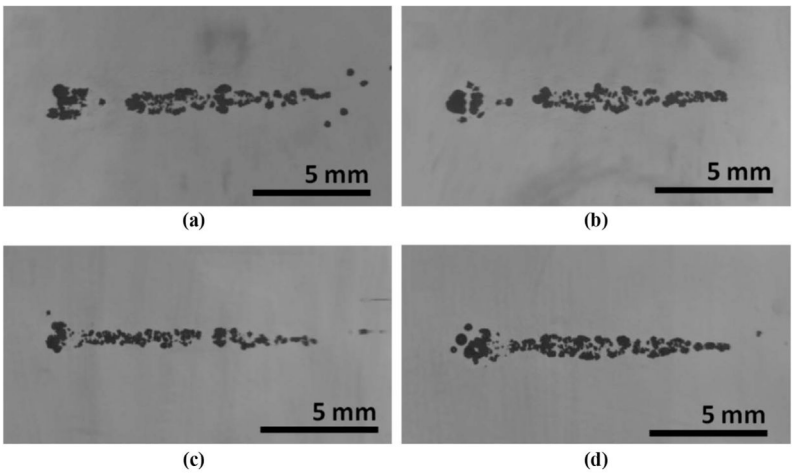

Fig. 6.

High-speed images of bubble clouds (shown as the dark clusters of dots) generated in a transparent agarose phantom: (a) in a free field, (b) with the rib phantom at 8 cm, (c) with the rib phantom at 4 cm, and (d) with the porcine ribs at 8 cm. Longitudinal planes are shown. Ultrasound propagation: left to right.

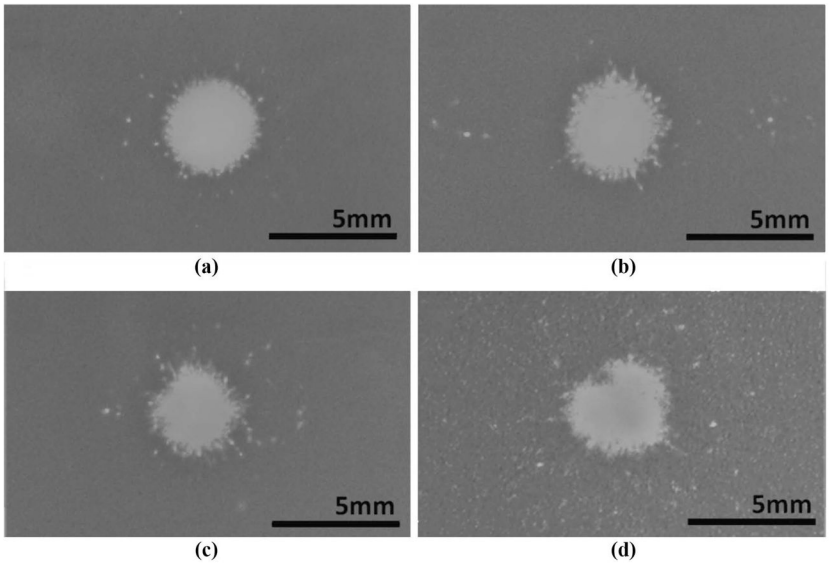

Fig. 7.

Transversal lesion patterns: (a) in a free field, (b) with the rib phantom positioned at 8 cm from the focus, (c) with the rib phantom at 4 cm, and (d) with porcine ribs at 8 cm. Lesions correspond to the visually clear areas surrounded by the darker background color of the red blood cell layer. Collateral damage was defined as the sum of all damage spots detected outside the continuous portion of the main lesion.

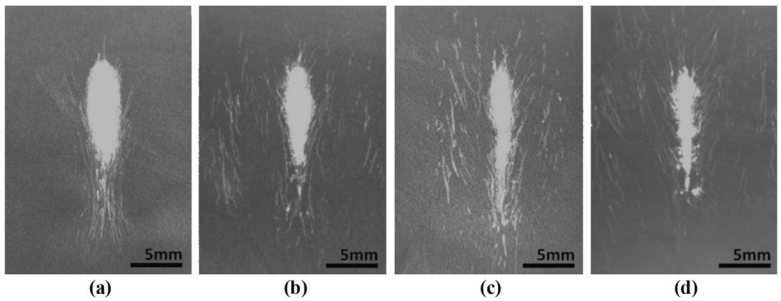

Fig. 8.

Representative longitudinal plane lesions: (a) in free field, (b) with the rib phantom at 8 cm, (c) with the rib phantom at 4 cm, and (d) with porcine ribs at 8 cm. The trailing paths created by the translation of marginal bubble nuclei were the cause of most of the collateral effects seen in the longitudinal plane. Ultrasound propagation: top to bottom.

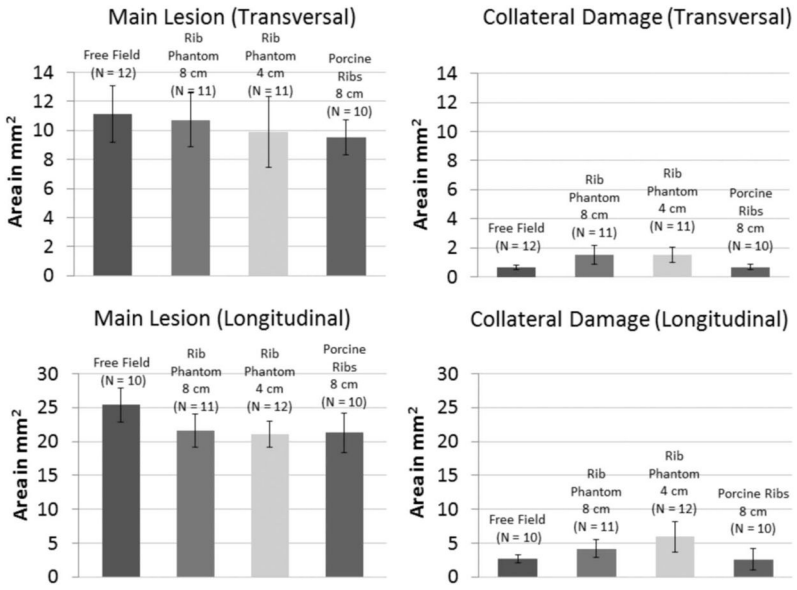

Fig. 9.

Main lesion dimensions and collateral damage on the transversal and longitudinal plane lesions generated in a free field and through the rib aberrators. Error bars correspond to plus or minus one standard deviation for each data set.

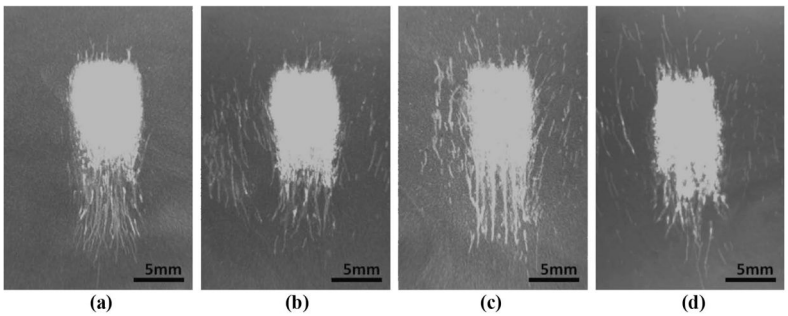

Fig. 10.
Lesions created by applying 5 adjacent treatments separated by 1 mm, covering a total zone of approximately 7 × 10 mm: (a) in a free field, (b) with the rib phantom at 8 cm, (c) with the rib phantom at 4 cm, and (d) with porcine ribs at 8 cm. Ultrasound propagation: top to bottom.